ROLL-BOND HEAT EXCHANGER (RHE) DESIGN AND APPLICATION TO A CHOCOLATE COOLING TUNNEL - A NUMERICAL STUDY

UDC:621.565:519.6
Original scientific paper https://doi.org/10.46793/adeletters.2023.2.4.4

Abdullah Sadık Tazegül[1*], Ömer Sinan Şahin[2], Osman Okumuşer[1]

[1]Tüfekçioğulları Machine Company R&D Center, Karaman City, Türkiye
[2]Konya Technical University, Faculty of Engineering and Natural Sciences, Department of Mechanical Engineering, Konya City, Türkiye

Abstract:
The snack sector has a significant market today. It is expected that the snacks will look as promised on the packaging and that the product will have no deformations or defects. The entire area of liquid chocolate-covered snack products entering the chocolate cooling tunnel must be cooled homogeneously. If all surfaces of the chocolate are not sufficiently cooled, a problem of sticking to the conveyor belt can occur. This study investigates the performance of roll-bond heat exchangers under different operating conditions to solve the snack sector's technical problems. For this purpose, a CAD model of a roll-bond heat exchanger is created. A steady-state heat transfer problem is established in the SolidWorks Flow Simulation environment, and the problem is solved numerically. The maximum, minimum, and average values of the fluid temperature, pressure difference, fluid velocity, and solid temperature distributions are calculated for different inlet velocities and temperatures. In addition, the standard deviations of the solid temperature values are calculated and evaluated. The results show that the roll-bond heat exchanger applies to the chocolate cooling tunnel and is much more efficient for heat transfer than the conventional design.

ARTICLE HISTORY

Received: 3 October 2023
Revised: 27 November 2023
Accepted: 29 December 2023
Published: 31 December 2023

KEYWORDS

Development of roll-bond heat exchanger, computational fluid dynamics, heat exchanger performance, industrial cooling tunnel, chocolate product cooling

1. INTRODUCTION

The most consumed sweet snacks today are chocolate-coated products. The high consumption of these coated products is due to the preference for the chocolate and sugar included in the chocolate. Chocolate-coated products can be realized as nougat, coconut, and cereal products such as hazelnuts, peanuts, energy bars, cakes, or wafers [1-3].

It can be said that chocolate is a generally preferred component of the sweet snack sector. For chocolate to change from solid to liquid without deterioration, it needs to be heated slowly and continuously, stirring at 40-45°C [2-5]. Chocolate, which liquefies after heating, is poured into molds to produce plain snack products or coated on different snack products (chocolate) to enrich the taste and appearance of the snack products. The liquid chocolate coating must be cooled to pass into the solid phase. The first part of the coating is completed by passing the snack product through a waterfall of hot chocolate, leaving a thin shell structure. This structure is then cooled slowly, and the encrusting process is completed. In the snack sector, many scientific studies have been conducted on the use of chocolate on various products, and the heating and cooling process of chocolate and different chocolate recipes have been obtained [2-4, 6]. In general, chocolates are heated up to 45°C,

*CONTACT: Abdullah Sadık Tazegül, e-mail: s.tazegul@nefamak.com.tr

and at temperatures above this value, chocolate loses its properties and deteriorates. Subsequently, the liquid chocolates need to be cooled to a temperature between 10-12°C (approximately 3 °C/min) for 9-12 minutes on average in order to solidify [2-4, 7]. If the liquid chocolate-coated products are cooled faster than the temperature values mentioned above, the products crystallize and adversely affect the quality (taste), which is called the eating profile [3, 8, 9]. Therefore, liquid chocolate should be cooled slowly and with minimal temperature differences [3, 4, 10]. Cooling tunnels are usually designed very long in order to cool liquid chocolate slowly [3, 4, 11]. After the sweet snack products are coated with liquid chocolate, they enter cooling tunnels further down the production line. The coated snack products that slowly move through the cooling tunnels are slowly cooled in the tunnel. In this process, the product covered with liquid chocolate, which moves in the cooling tunnel with PVC tapes or other transport mechanisms, is cooled by heat transfer and air-cooled to 10-15°C [3-4]. The chocolate mentioned above cooling times in the tunnel (9-12 minutes) vary for each chocolate recipe [3, 4]. For example, the cooling time for a milk chocolate recipe can be up to 12 minutes. The chocolate-coated snack products travel on a PVC tape in the cooling tunnel and the pre-cooled air transfers heat by convection.

The lower parts of the products cannot sufficiently transfer heat with cold air since the lower parts of the snack products coated with liquid chocolate are in contact with the PVC tape. For this reason, all parts of the products cannot be cooled homogeneously, and the liquid chocolate in the lower parts of the products adheres to the PVC tape, and the integrity of the coating on the product is disrupted [12]. Many studies have been conducted in the literature on product integrity, product quality, and the effect of production machinery on food and similar problems [13-18]. In order to prevent non-cooling problems experienced in the lower parts of chocolate-coated products, the surface in contact with the product's underside must also be cooled.

For this purpose, it is also possible to circulate the cooled air under the products to achieve cooling on the bottom surfaces. However, the Roll-bond heat exchanger, which is used for heating/cooling with the help of water in areas such as solar panels and refrigerators, is considered to be a solution to overcome this problem since the specific heat of water is about six times higher than the specific heat of air. The studies on this subject [19, 20] also support this idea. A roll-bond is a structure formed by opening channels to allow liquid flow between metal plates brought together. The product can be cooled by providing water flow through the hollow water chamber and the water chamber filled with obstacles (Roll-bond), as shown in Fig. 1 [20, 21].

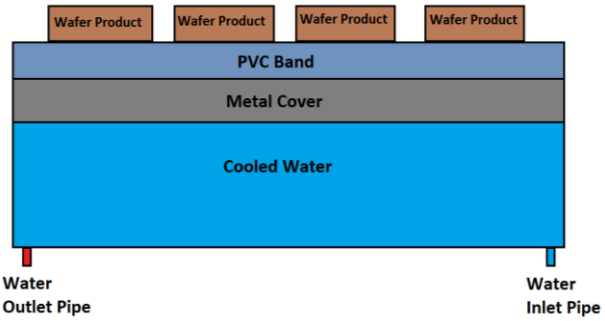

Fig.1. Schematic description of Roll-bond cooling system

It is aimed to realize homogeneous cooling by placing this system under PVC belts in cooling tunnels. It has been reported that it is possible to achieve similar cooling efficiency with conventional cooling methods [22]. The main research question related to the roll-bond system is to provide sufficient interaction time and turbulent flow between the cooled water and metallic plates to ensure homogeneous and high heat transfer. For this purpose, turbulence is increased by placing flow-deflecting obstacles (turbulators) inside the structure's chamber.

This study is about the numerical modeling of the Roll-bond heat exchanger design to be built under the belt of the chocolate cooling tunnel for the problem of non-cooling of the lower region of hot chocolate coated snack products (not passing to solid phase) in chocolate cooling tunnels. In this study, two different cold-water chambers with the exact dimensions were designed to provide heat transfer under the conveyor belt that advances the products to be cooled in the chocolate cooling tunnel. The aim of the study is to investigate the numerical effects of two different cold-water chambers, the effect of deflecting turbulators on the fluid velocity, fluid temperature, inlet-outlet pressure differences, and the temperature distribution on the sheet-metal plate on the two different cold-water chambers.

2. MATERIALS AND METHOD

In this study, two cold water reservoir designs with different designs were analyzed using the computational fluid dynamics (CFD) method

(Solidworks Flow Simulation software), and criteria were determined to compare the flow and heat transfer results. In order to be analyzed in CFD software, criteria were determined to compare the results of the average velocity of the fluid, inlet-outlet pressure differences to ensure fluid movement, and temperature differences (ΔT) created by the sheet-metal plate contacting the cold-water reservoir. Firstly, a roll-bond type water reservoir and a conventional type water reservoir (no obstruction in the inner chamber) used in different areas were designed with the exact external dimensions. The two different water reservoir designs were made using SolidWorks 3D software and are presented in Fig. 2. Table 1 shows the input parameters to the CFD software.

The dimensions of the sheet metal plate contacting the roll-bond type heat exchanger water tank and the conventional type water tank are 2772x1460x5 mm, which are widely used in industrial applications (Fig. 3).

Table 1. Input parameters to the CFD software [23]

Parameter	Value
Density ($\boldsymbol{\rho}$)	8000 kg/m^3
Heat conduction coefficient ($\boldsymbol{k}$)	16 W/m·K
Specific heat ($\boldsymbol{C_p}$)	500 J/(kg·K)
The initial temperature ($\boldsymbol{T_i}$)	20 °C
The fluid initial temperature ($\boldsymbol{T_{i_f}}$)	5 °C
The gravity acceleration (g)	9.81 m/s^2
The total number of mesh elements of the conventional type water reservoir fluid	3.2 million
The total number of solid mesh elements	3.2 million
The total inlet pressure of the fluid ($\boldsymbol{P_i}$)	3 Bar
The pressure at the outlet of the fluid ($\boldsymbol{P_O}$)	3 Bar
The heat transfer coefficient ($\boldsymbol{h}$)	17 W/m^2·K
The external air temperature ($\boldsymbol{T_e}$)	28 °C
The metal roughness value ($\boldsymbol{R_a}$)	0.01 µm
Turbulence intensity ($\boldsymbol{I}$)	2%
Turbulence length ($\boldsymbol{L}$)	0.00072 m

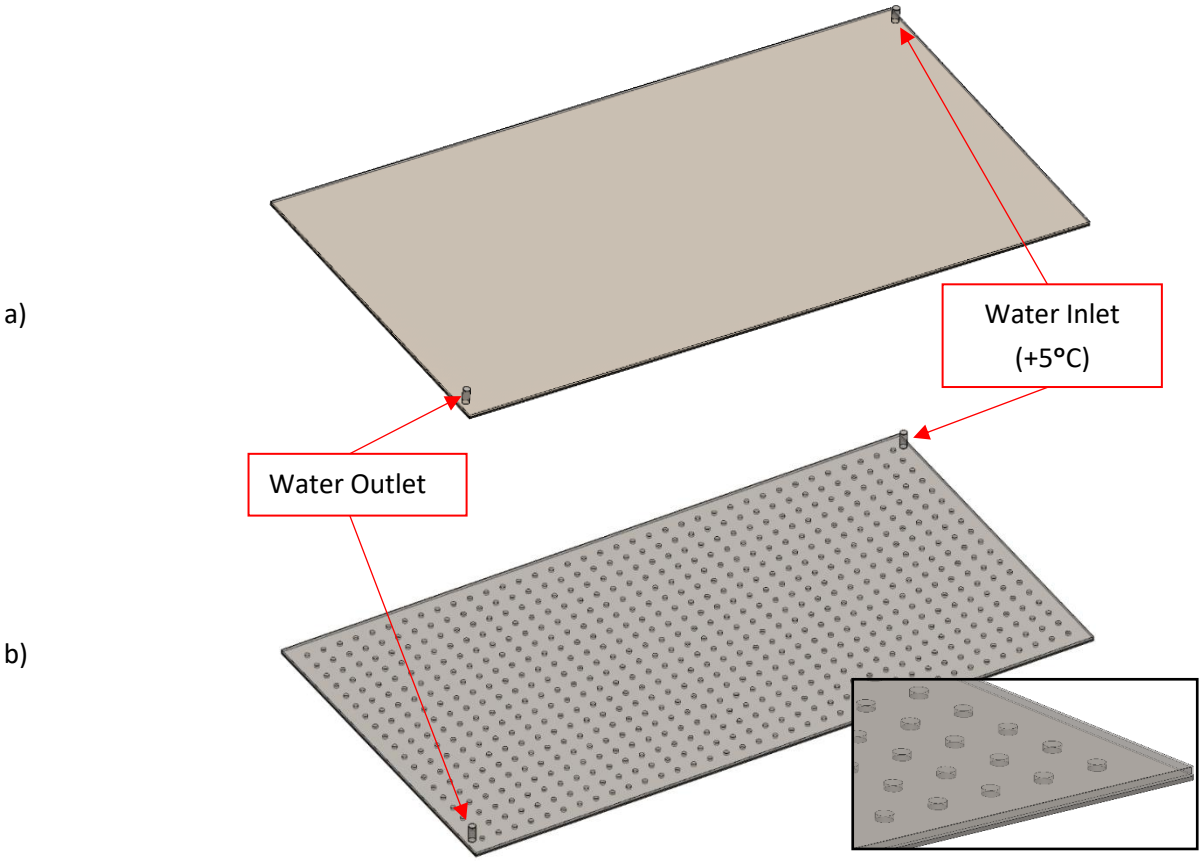

Fig. 2. Water tank: a) Conventional type, and b) Roll-bond type

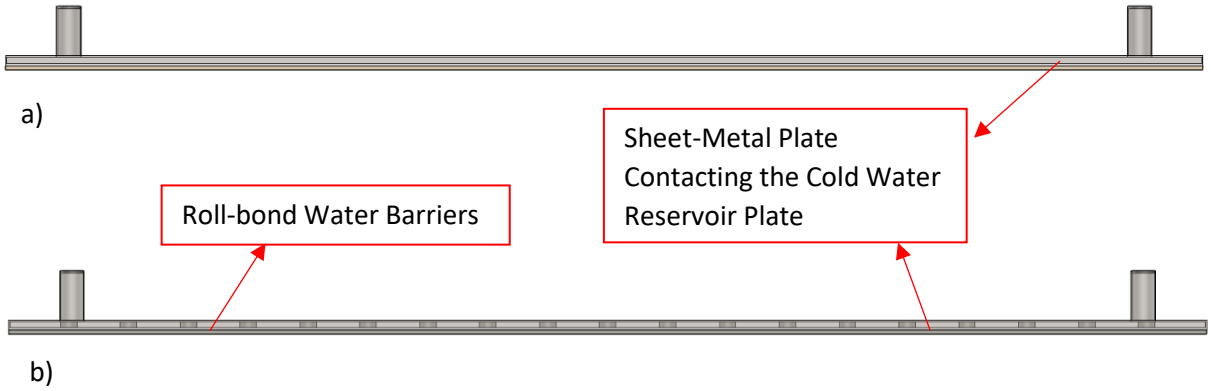

Fig.3. Water reservoir cross-sectional images: a) Conventional type water tank, and b) Roll-bond type

All components used in the design are assumed to be made of AISI 304 stainless. Numerical solutions were obtained by SolidWorks Flow Simulation CFD software under identical boundary conditions. The gravity acceleration was determined in the +Z direction. Only the laminar flow type was chosen by allowing heat conduction in solids. The heat transfer coefficient was selected as the outer wall thermal condition. In both analyses, flow characteristics, turbulence and laminar were selected and automatic determination of the flow type was requested from the software.

The analyses were analyzed as a steady state. Equation 1 gives the Navier-Stokes equation for incompressible homogeneous fluids in the x, y and z axes for fluid regions [24]. If the fluid is homogeneous and incompressible; $\frac{\partial \rho}{\partial t}$=0. This means that the density does not change with time.

$$\rho\left(\frac{\partial u}{\partial t}+u\frac{\partial u}{\partial x}+v\frac{\partial u}{\partial y}+w\frac{\partial u}{\partial z}\right) = P-\frac{\partial P}{\partial x} + \mu\left(\frac{\partial^2 u}{\partial x^2}+\frac{\partial^2 u}{\partial y^2}+\frac{\partial^2 u}{\partial z^2}\right)$$

$$\rho\left(\frac{\partial v}{\partial t}+u\frac{\partial v}{\partial x}+v\frac{\partial v}{\partial y}+w\frac{\partial v}{\partial z}\right)=Q-\frac{\partial P}{\partial y}+\mu\left(\frac{\partial^2 v}{\partial x^2}+\frac{\partial^2 v}{\partial y^2}+\frac{\partial^2 v}{\partial z^2}\right)$$

$$\rho\left(\frac{\partial w}{\partial t}+u\frac{\partial w}{\partial x}+v\frac{\partial w}{\partial y}+w\frac{\partial w}{\partial z}\right)=Q-\frac{\partial P}{\partial z}+\mu\left(\frac{\partial^2 w}{\partial x^2}+\frac{\partial^2 w}{\partial y^2}+\frac{\partial^2 w}{\partial z^2}\right) \quad (1)$$

In the equations, $P=\rho g_x$, $Q=\rho g_y$, P and Q represent external forces.

In Equation 1, v(u,v,w) denotes the velocity values and u,v and w denote the velocity values in the x, y and z axes. P is the pressure, ∂t is the change with time, ρ is the fluid density, μ is the dynamic fluid viscosity and g is the gravity. These equations state that the product of mass and acceleration is proportional to the force acting on a fluid particle, preserving the continuity of mass and momentum. In Equation 2, the turbulence conservation law is given for laminar, turbulent and transitional flows of homogeneous fluids following the $k-\varepsilon$ turbulence model with damping function realized by Lam-Bremhorst [25].

$$\frac{\partial \rho k}{\partial t}+\frac{\partial \rho k u_i}{\partial x_i}=\frac{\partial}{\partial x_i}\left(\left(\mu+\frac{\mu_t}{\sigma_k}\right)\frac{\partial k}{\partial x_i}\right)+\tau_{ij}^R\frac{\partial u_i}{\partial x_j}-\rho\varepsilon+\mu_t P_b$$

$$\frac{\partial \rho \varepsilon}{\partial t}+\frac{\partial \rho \varepsilon u_i}{\partial x_i}=\frac{\partial}{\partial x_i}\left(\left(\mu+\frac{\mu_t}{\sigma_\varepsilon}\right)\frac{\partial \varepsilon}{\partial x_i}\right)+C_{\varepsilon 1}\frac{\varepsilon}{k}\left(f_1\tau_{ij}^R\frac{\partial u_i}{\partial x_j}+C_B\mu_t P_B\right)-f_2 C_{\varepsilon 2}\frac{\rho\varepsilon^2}{K}$$

$$\tau_{ij}=\mu s_{ij},\qquad \tau_{ij}^R=\mu_t s_{ij}-\frac{2}{3}\rho k\delta_{ij},\quad s_{ij}=\frac{\partial u_i}{\partial x_j}+\frac{\partial u_j}{\partial x_i}-\frac{2}{3}\delta_{ij}\frac{\partial u_k}{\partial x_k}$$

$$P_B=-\frac{g_i}{\sigma_B}\frac{1}{\rho}\frac{\partial \rho}{\partial x_i} \quad (2)$$

The constants in the $k-\varepsilon$ model is $C_\mu=0.009$, $C_{\varepsilon 1}=1.44$, $C_{\varepsilon 2}=1.92$.

The empirical constants in the turbulence model are $\sigma_k=1$, $\sigma_\varepsilon=1.3$, $\sigma_B=0.9$, $P_B>0$ for the case $C_B=1$, $P_B<0$ for the case $C_B=0$.

Turbulent viscosity $\mu_t=f_\mu.\frac{C_\mu\rho k^2}{\varepsilon}$ and Lam and Berhorst's damping function:

$$f_\mu=\left(1-e^{-0.0025R_y}\right)^2\cdot\left(1+\frac{20.5}{R_t}\right), \quad (3)$$

Y distance from wall to point, Lam and Berhorst's f_1 and f_2 damping function:

$$f_1=1+\left(\frac{0.05}{f_\mu}\right)^3, \quad (4)$$

$$f_2 = 1 - e^{-R_t^2}, \quad (5)$$

ε is the isotropic dissipation rate, μ the dynamic fluid viscosity, ρ the fluid density, u_i and u_j the tensors for velocities on the x, y axes, k the turbulence energy, the lower notation X_t turbulence, Reynolds Numbers for R_t, R_y turbulence, C is the turbulent model constant, ∂t is the time-dependent variation, f_1, f_2 is the turbulent model function, σ_k is the diffusion Prandtl value (a dimensionless quantity relating the viscosity of a fluid to the thermal conductivity) for the turbulence energy. Equation 6 gives the equations used for thermal convection in liquid regions and Equation 7 for thermal conduction in solid regions [26].

In thermal convection in liquid regions,

$$q_i = \left(\frac{\mu}{Pr} + \frac{\mu_t}{\sigma_c}\right)\frac{\partial h}{\partial x_i}, \; i = 1,2,3 \quad (6)$$

The contents $\sigma_c = 0.9$, Pr Prandtl number and h is the thermal enthalpy.

In heat conduction in solid media,

$$\frac{\partial \rho e}{\partial t} = \frac{\partial}{\partial x_i}\left(\lambda_i \frac{\partial T}{\partial x_i}\right) + \theta_H \quad (7)$$

ρe is heat transfer value, q_i is heat flux, μ_t is turbulent viscosity, μ is dynamic fluid viscosity, ρ is fluid density, specific internal energy $e = cT$, c is the specific heat, T is the temperature, θ_H is the specific heat dissipation concerning the velocity, ∂T is the thermal boundary layer thickness, ∂x_i is the change in the x-axis, λ_i is the eigenvalues of the thermal conductivity tensor. As a result of the analysis, the heat transfer results with the velocity of the cold fluid passing through two different water reservoirs and on the sheet-metal plate in contact with the water reservoir were obtained.

3. RESULT AND DISCUSSIONS

3.1 Fluid Zone

The results were analyzed to see the velocity data of the fluid (cold water) passing through two different water chambers and the fluid temperature changes. Fig.4 shows the results of the change in the water velocity due to two different designs: conventional-type water reservoirs and Roll-bond-type water reservoirs. In Fig. 4, the maximum velocity value of the fluid in the conventional type water reservoir is 11.741 m/s and the minimum velocity value is 0.0001335 m/s. In Fig. 4, the maximum velocity value of the fluid in the roll-bond type water reservoir is 11.190 m/s and the minimum velocity value is 0.003 m/s.

Looking at the maximum fluid velocity values for the two different designs in Fig. 4, it is seen that the Roll-bond type water reservoir is approximately 5% lower than the conventional water reservoir. It is clearly seen that the Roll-bond type water reservoir is approximately 22.5 times higher than the conventional type water reservoir when looking at the minimum fluid velocity values in two different designs. This is due to the fact that the large vortices of the conventional type water reservoir gather at certain points and cause stagnation in the corner regions. The fact that the velocity of the fluid formed in the corner regions of the conventional type water reservoir is close to stagnation is an indication that there are more dead zones. Looking at the average fluid velocities of the two different designs in Fig. 4, it is realized that the Roll-bond type water reservoir (0.741502) has a 3.5% lower velocity than the conventional type water reservoir (0.768019 m/s) and the Roll-bond type water reservoir has a more homogeneous velocity distribution and much fewer dead zones than the other design. This is also confirmed by the low standard deviation, as shown in Fig. 4.

Fig. 5 shows the pressure change results of the conventional type water reservoir and Roll-bond type water reservoirs depending on two different designs. In Fig. 5, the maximum pressure value of the fluid in the conventional type water reservoir is 293382.12 Pa, and the minimum pressure value is 116503.96 Pa. In Fig. 5, the maximum pressure value of the fluid in the roll-bond type water reservoir is 290595.11 Pa, and the minimum pressure value is 107891.08 Pa. Looking at the maximum fluid pressure values in two different designs in Fig. 5, it is seen that the Roll-bond type water reservoir is approximately 1% lower than the conventional type water reservoir. Looking at the minimum fluid pressure values in the two different designs, it is seen that the Roll-bond type water reservoir is at a pressure approximately 8% lower than the conventional type water reservoir. Fig. 6 shows the temperature change results of the conventional type water reservoir and Roll-bond type water reservoirs depending on two different designs.

Fig. 6 shows that the maximum temperature of the fluid in the conventional type water reservoir is 5.85°C and the minimum temperature is 5°C. In Fig. 6, the maximum temperature of the fluid in the Roll-

bond type water tank is 5.23°C and the minimum temperature is 5°C. In Fig. 6, the average fluid value in the conventional type water reservoir was 222008.931 Pa and the average fluid value in the Roll-bond type water reservoir was 221924.134 Pa.

Looking at the fluid temperatures of the two different designs, it was realized that the maximum temperature values were almost equal. However, it was clearly realized that the fluid temperature of the Roll-bond type water reservoir exhibited a more homogeneous distribution.

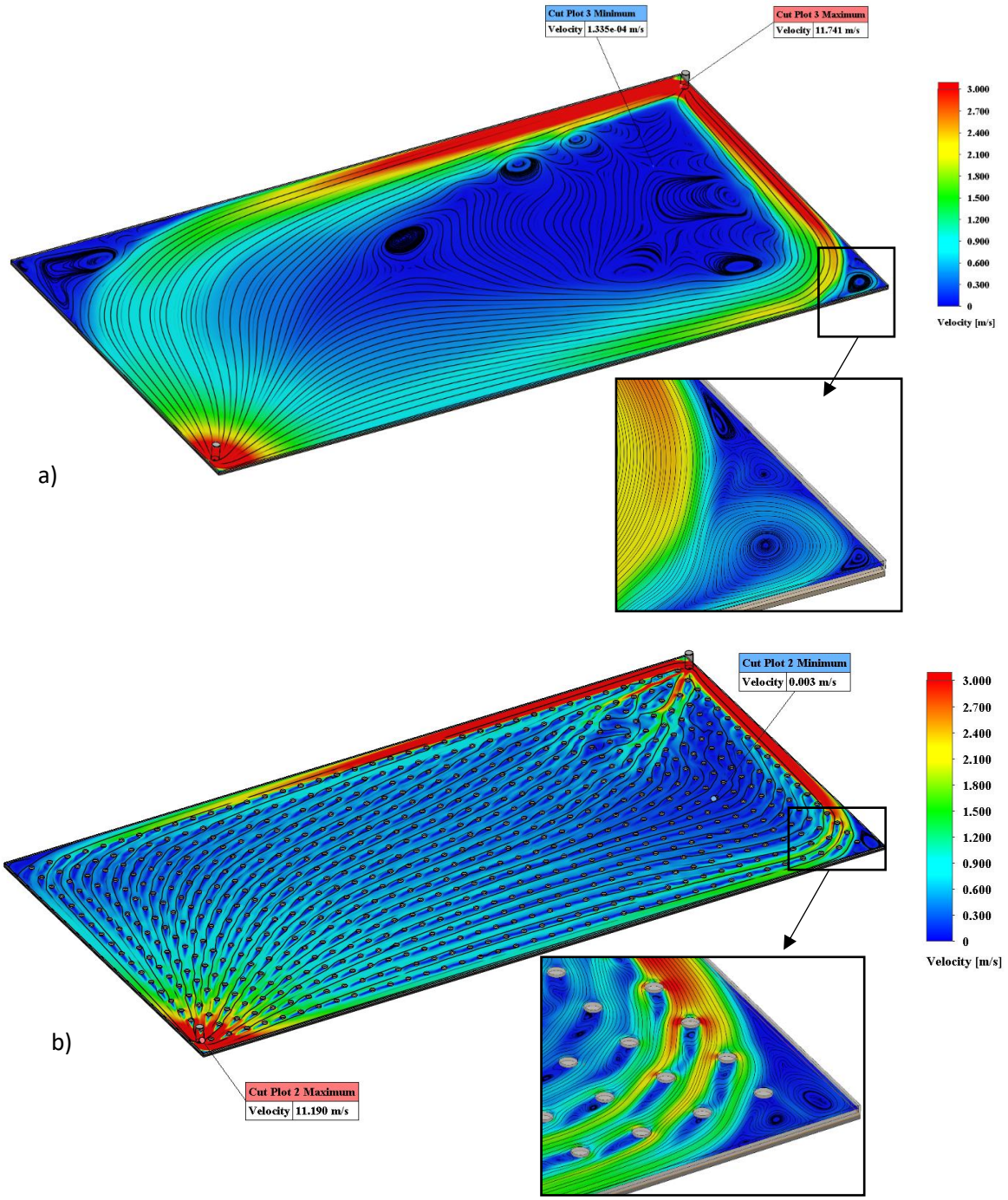

Fig.4. Water velocity distribution: a) Conventional type water tank, and b) Roll-bond type water tank

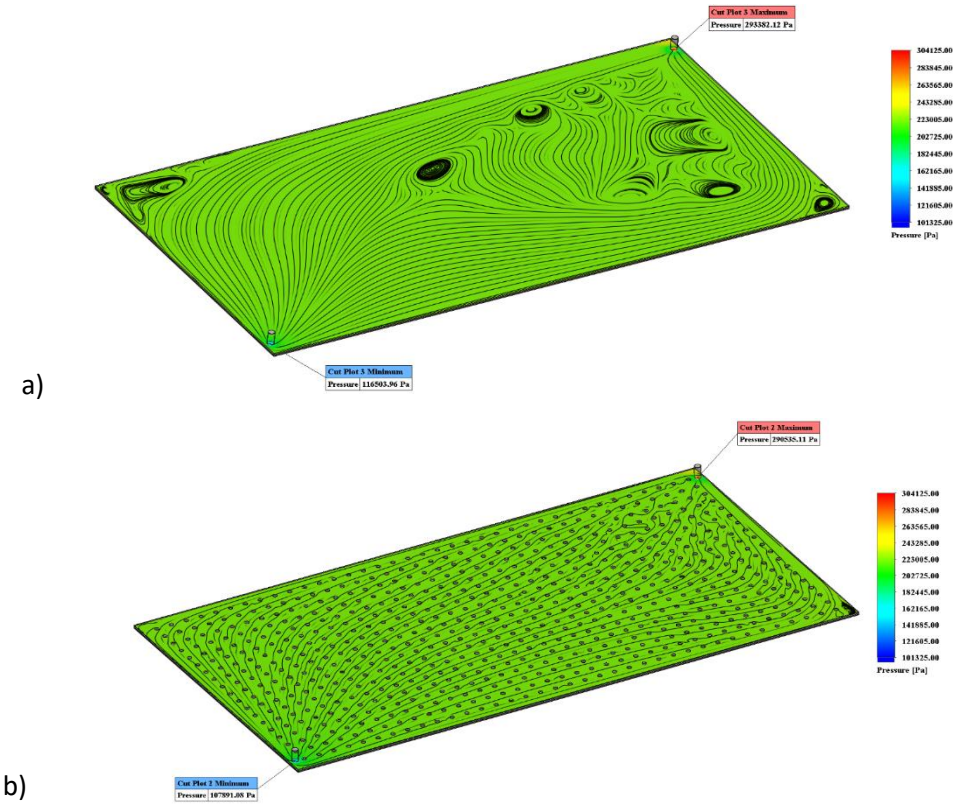

Fig. 5. Water pressure distribution: a) Conventional type water tank, and b) Roll-bond type water tank

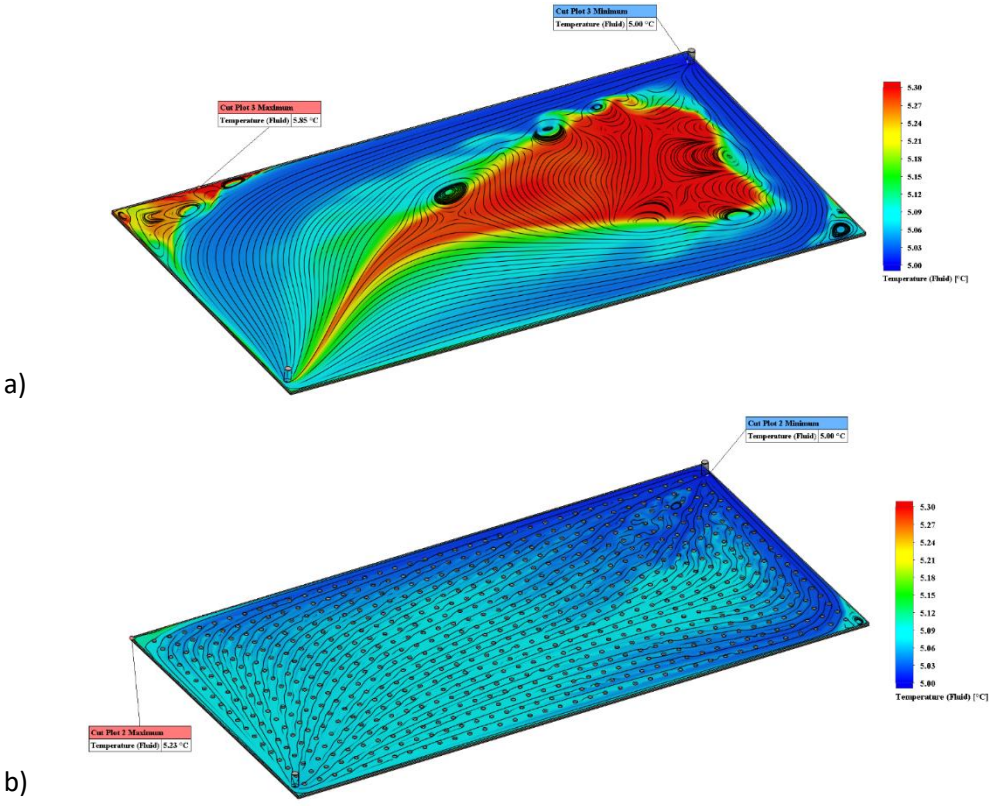

Fig. 6. Temperature distribution of water depending on two different designs: a) Conventional type water tank, and b) Roll-bond type water tank

3.2 Solid Zone

Fig. 7 shows the temperature change results of the sheet-metal plates contacting the conventional type water tank and Roll-bond type water tank according to the heat transfer with water. In Fig. 7, the maximum temperature value is 7.14°C and the minimum temperature value is 5.19°C due to the heat transfer of the sheet-metal plate contacting the conventional water tank with water. In Fig. 7, the maximum temperature value is 6.56°C and the minimum temperature value is 5.19°C due to the heat transfer of the sheet-metal plate contacting the roll bond type water tank with water.

In order to see the temperature distribution received by the sheet-metal plates contacting the water reservoirs with two different internal designs, temperature data were taken from 5012 separate points. Fig. 8 shows the 5012 temperature points determined on the sheet metal plates contacting the conventional type water reservoir and Roll-bond type water reservoirs.

Table 2 shows the maximum temperature, minimum temperature, average temperature, standard deviation values taken from 5012 separate points on the sheet-metal plates contacting the water tank with two different internal designs.

Table 2. Numerical values obtained from metal plate (5012 discrete points)

Parameter	Konventional	Roll-bond
Maximum Solid Temperature (°C)	7.14	6.56
Minimum Solid Temperature (°C)	5.19	5.19
Average Solid Temperature (°C)	8.86	5.502
Temperature Standard Deviation	0.3385	0.0193

In Table 2, the maximum temperature value of the sheet-metal plate contacting the conventional type water tank was 7.14°C, the minimum temperature was 5.19°C, the average temperature was 5.86°C and the standard deviation was 0.3385. In Table 2, the maximum temperature value of the sheet-metal plate contacting the roll-bond type water tank was 6.56°C, the minimum temperature was 5.19°C, the average temperature was 5.502°C and the standard deviation was 0.0193.

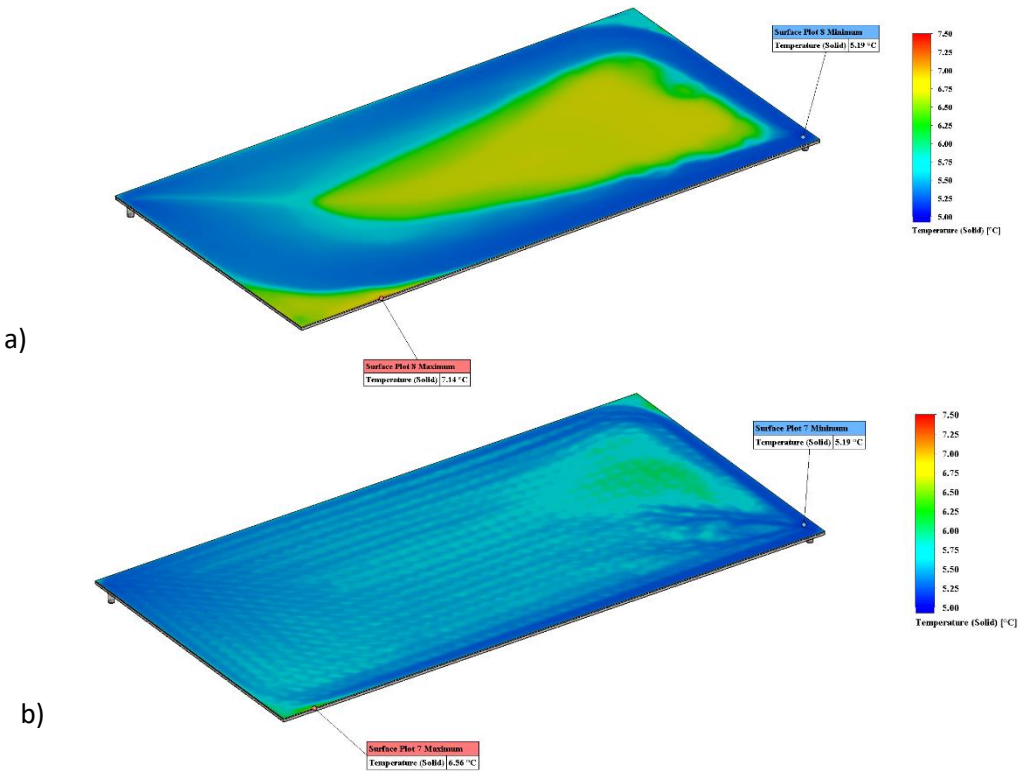

Fig. 7. Design-dependent temperature variation of sheet-metal plates in contact with two different water reservoirs: a) Conventional type water tank, and b) Roll-bond type water tank

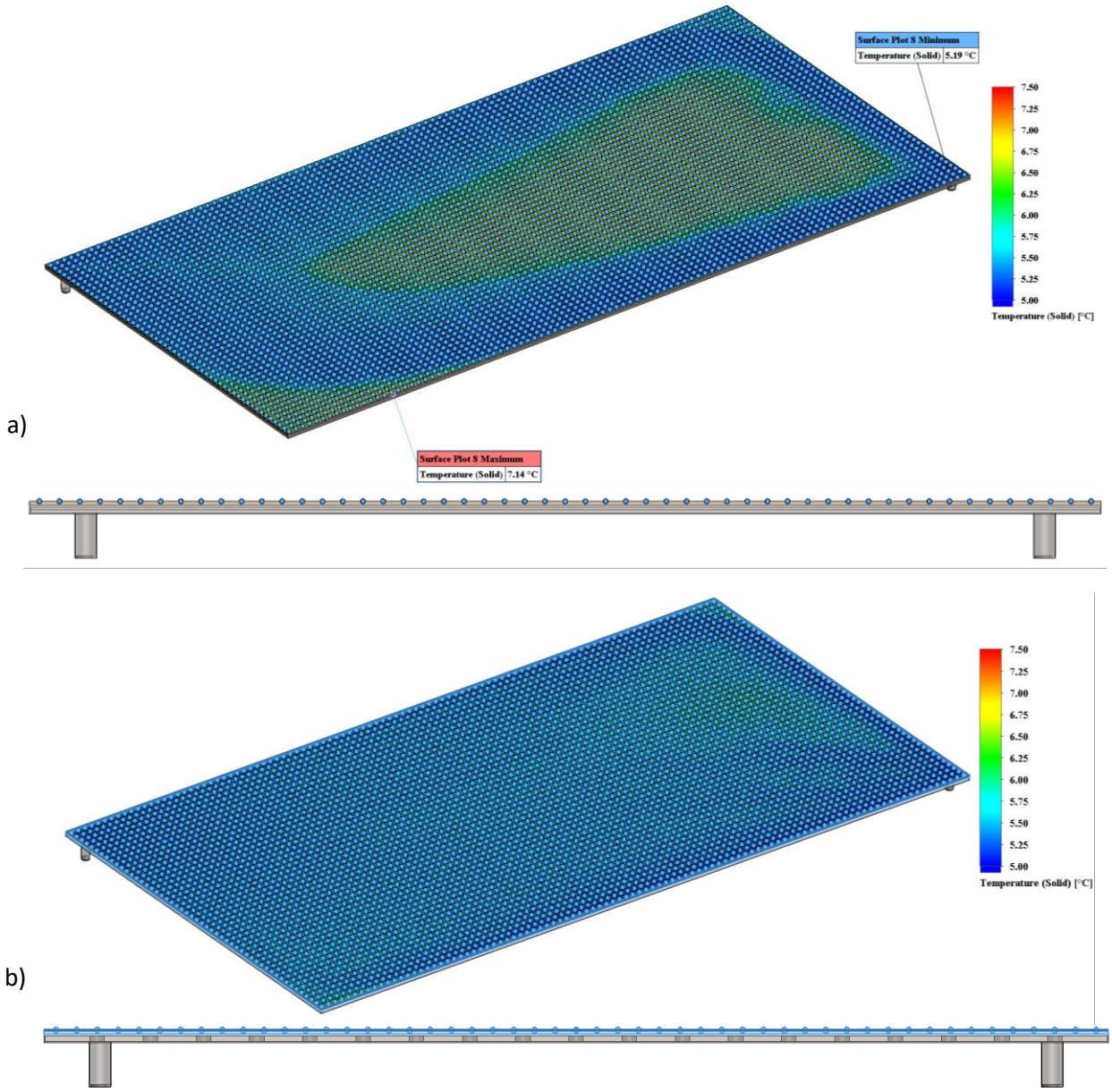

Fig. 8. There are 5012 temperature points determined on the sheet-metal plates in contact with the: a) conventional type water tank, and b) Roll-bond type water tanks

Fig. 9 shows the metal temperatures and standard deviation variation values of the temperatures taken from 5012 separate points on the sheet-metal plates in contact with two different water reservoirs. In Fig. 9, the line drawn between the minimum temperature points for both designs shows a trend close to flat. In Fig. 9, the line drawn between the same case average temperature points for both designs showed a trend close to flat. However, both designs have an excess variation of 0.58°C between the maximum temperature points. Fig. 9 shows that the standard deviation of the temperature data from 5012 separate points for both designs is more than 17.5 times higher.

4. CONCLUSION

This study is concerned with the numerical modeling of the roll-bond heat exchanger design to be built under the chocolate cooling tunnel PVC belt for the problem of non-cooling (non-solid phase) of the lower zone of hot chocolate coated snack products. Depending on the cold-water inner chamber design, the effects of fluid velocity, fluid temperature, inlet-outlet pressure differences and temperature distribution on the sheet-metal plates in contact with the water chamber were

investigated. The results obtained at the end of the analysis are listed below:

- The roll-bond design has very few dead flow regions compared to the conventional design. Throughout the design, the controlled distribution of vortices (with turbulators) resulted in a temperature distribution about 4 times more homogeneous.
- The fact that the pressure is 7.5% lower in the roll-bond type design compared to the conventional type design is considered an insignificant loss considering a homogeneous temperature distribution.
- It is clear from the numerical data that the Roll-bond type design is more suitable in many respects for chocolate-coated snack products moving in the chocolate cooling tunnel.
- Finally, a separate study can be conducted to find the optimum shape and size of the turbulators by changing the shape and size of the turbulators formed in the roll-bond type design through the effects of fluid velocity, fluid pressure differences, fluid temperature distribution, and solid temperature distribution.

ACKNOWLEDGEMENT

This study was supported by the Ministry of İndustry and Technology of The Republic of Türkiye R&D Projects (Project No: 152011045). We would like to thank Tüfekçioğulları Machine (NEFAMAK) Company and the Ministry of Industry and Technology of The Republic of Türkiye for initiating the project.

REFERENCES

[1] M.J. Bean, 17 - Manufacturing Processes: Enrobing, In: G. Talbot (Ed.), Woodhead Publishing Series in Food Science, Technology and Nutrition. Science and Technology of Enrobed and Filled Chocolate, Confectionery and Bakery Products. *Woodhead Publishing*, 2009: 362-396. https://doi.org/10.1533/9781845696436.3.362

[2] K.F. Tifenbacher, The technology of wafers and waffles II: Recipes, product development and know-how. *Elsevier*, Netherlands, 2018.

[3] K.F. Tifenbacher, The Technology of Wafers and Waffles I: Operational Aspects. *Elsevier*, Netherlands, 2017.

[4] S.T. Beckett, M.S. Fowler, G.R. Ziegler, Beckett's Industrial Chocolate Manufacture and Use. *John Wiley &Sons*, Hoboken, 2017.

[5] B.J.D. Le Reverend, Modelling of the phase change kinetics of cocoa butter in chocolate and application to confectionary manufacturing, (Ph.D. Thesis). *Faculty of Chemical Engineering, University of Birmingham,* England, 2010.

[6] M. Rusconi, A. Conti, Theobroma Cacao L., The Food of The Gods: A Scientific Approach Beyond Myths and Claims. *Pharmacological Research,* 61(1), 2010: 5-13. https://doi.org/10.1016/j.phrs.2009.08.008

[7] H. Tewkesbury, A.G.F. Stapley, P.J. Fryer, Modelling Temperature Distributions in Cooling Chocolate Moulds. *Chemical Engineering Science*, 55(16), 2000: 3123-3132. https://doi.org/10.1016/S0009-2509(99)00578-3

[8] N. Baichoo, The Effect of Rapid Cooling on the Fat Phase of Chocolate (Ph.D. Thesis). *Faculty of Science, University of Nottingham*, England, 2007.

[9] E.O. Afoakwa, A. Paterson, M. Fowler, J. Vieira, Particle Size Distribution and Compositional Effects on Textural Properties and Appearance of Dark Chocolates. *Journal of Food Engineering*, 87(2), 2008: 181-190. https://doi.org/10.1016/j.jfoodeng.2007.11.025

[10] Ö.S. Toker, H.R. Pirouzian, N. Konar, D.G. Polat, βv Seeding as An Alternative Pre-Crystallization Technique in Synbiotic Milk Chocolate Production. *Gıda*, 43(3), 2018: 422-431. https://doi.org/10.15237/gida.GD18020

[11] M.S. Amri, M.F. Basar, M.F. Yaakub, A.M. Kamarul, M. BinSam, An Integrated Cooling Tunnel for Preventing the Breakage of Chocolate Snack Bars. International Journal of Engineering Trends and Technology, 69(9), 2021: 66-72. https://doi.org/10.14445/22315381/IJETT-V69I9P209

[12] M.P. Gray, Moulding, Enrobing and Cooling Chocolate Products. In: S.T. Beckett, M.S. Fowler, G.R. Ziegler (Ed.). Beckett's Industrial Chocolate Manufacture and Use. *John Wiley & Sons*, 2017: 356-399. https://doi.org/10.1002/9781118923597.ch14

[13] R. Meral, İ. S. Doğan, Evaluation of Marketed Wafers in Terms of Quality and Ingredients.

Yuzuncu Yıl University Journal of Agricultural Sciences, 14(2), 2004: 65-71.

[14] M. Bitkin, A.S. Tazegül, M. Mayda, Quality Assessment of Wafer Oven Products by Image Processing. *Proceedings - 20 National Machine Theory Symposium*, 15 September 2021, Diyarbakır, Türkiye, pp.338-345.

[15] R. Huber, G. Kalss, R. Schoenlechner, Waffle Production: Influence of Baking Plate Material on Sticking of Waffles. *Journal of Food Science*, 82(1), 2017: 61-68. https://doi.org/10.1111/1750-3841.13562

[16] O.S. Sahin, M.H. Aksoy, A.S. Tazegul, Numerıcal Investıgatıon of Thermal and Mechanıcal Behavıor of Wafer Mold. *X International Conference Industrial Engineering and Environmental Protection (IIZS 2020)*, 8-9 October 2020, Zrenjanin, Serbia, pp.62-69.

[17] A. Szpicer, W. Bińkowska, I. Wojtasik-Kalinowska, S.M. Salih, A. Półtorak, Application of computational fluid dynamics simulations in food industry. *European Food Research and Technology*, 249(6), 2023: 1411-1430. https://doi.org/10.1007/s00217-023-04231-y

[18] A. Ambaw, T. Fadiji, U.L. Opara, Thermo-mechanical analysis in the fresh fruit cold chain: A review on recent advances. *Foods*, 10(6), 2021: 1357. https://doi.org/10.3390/foods10061357

[19] X. Sun, J. Wu, Y. Dai, R. Wang, Experimental Study on Roll-Bond Collector/Evaporator with Optimized-Channel Used in Direct Expansion Solar Assisted Heat Pump Water Heating System. *Applied Thermal Engineering*, 66(1-2), 2014: 571-579. https://doi.org/10.1016/j.applthermaleng.2014.02.060

[20] E. Cerit, Rollbond Heat Exchangers. *Engineer & the Machinery Magazine*, 54(646), 2013: 12-21.

[21] L. Deng, Y. Li, P. Xu, Z. Chen, W. Zhou, B. Li, Fabrication and Thermal Performance of a Novel Roll-Bond Flat Thermosyphon. *Applied Thermal Engineering*, 181, 2020: 115959. https://doi.org/10.1016/j.applthermaleng.2020.115959

[22] X.-H. Han, Q. Wang, Y.-G. Park, C. T'Joen, A. Sommers, A. Jacobi, A review of Metal Foam and Metal Matrix Composites for Heat Exchangers and Heat Sinks. *Heat Transfer Engineering*, 33(12), 2012: 991-1009. https://doi.org/10.1080/01457632.2012.659613

[23] https://asm.matweb.com/search/SpecificMaterial.asp?bassnum=mq304a (Accessed: 20 June 2023).

[24] S.R. Bistafa, On the Development of the Navier-Stokes Equation by Navier. *Revista Brasileira de Ensino de Física*, 40(2), 2018: e2301. https://doi.org/10.1590/1806-9126-RBEF-2017-0239

[25] C.K.G. Lam, K. Bremhorst, A Modified Form of the k-ε Model for Predicting Wall Turbulence. *Journal of Fluids Engineering*, 103(3), 1981: 456-460. https://doi.org/10.1115/1.3240815

[26] S. Patankar, Numerical Heat Transfer and Fluid Flow. *CRC Press*, Boca Raton, USA, 2018. https://doi.org/10.1201/9781482234213